RESEARCH ARTICLE

INTERNATIONAL RESEARCH JOURNAL OF MULTIDISCIPLINARY TECHNOVATION

Asian Research Association

DOI: 10.54392/rjmt2424

Synergistic Analysis of Hydrothermally Synthesized PANI-GO: MnO_2/MoO_3 Nanocomposites for Enhanced Structural and Supercapacitor Performance

R. Kalpana [a,*], P. Subbramaniyan [a]

[a] Department of Chemistry, Thiruvalluvar Govt. Arts College, Rasipuram, Namakkal-637401, Tamil Nadu, India

*Corresponding Author Email: sivaprakasamme@gmail.com

DOI: https://doi.org/10.54392/irjmt2424

Received: 04-01-2024; Revised: 27-01-2024; Accepted: 06-02-2024; Published: 15-02-2024

Abstract: This study explores the potential of PANI-GO:MnO_2/MoO_3 nanocomposites as high-performance supercapacitors, addressing the increasing energy storage demands in portable electronics devices. By varying the amount of polyaniline (PANI) alongside a ternary composite of GO/MnO_2/MoO_3, the present study investigates their combined influence on electrochemical performance. XRD analysis confirmed the hexagonal phase with an average particle size of 19 nm, and FTIR analysis showed the functional groups associated with the title compound. FESEM images demonstrated the leaf-like structures, and the EDAX spectrum confirmed the presence of Mn and Mo elements in the as-prepared samples. Electrochemical analysis showed a maximum capacitance of 596 F/g. The unique blend of graphene, polyaniline, and ternary metal oxides in these nanocomposites holds great promise for advanced supercapacitors. The research aims to understand how different levels of polyaniline impact the overall composition, providing insights into the synergies between these components and their effects on energy storage capabilities.

Keywords: Super capacitors, Graphene Oxide, Ternary Metal Oxides, Charge/Discharge Rates

1. Introduction

In today's rapidly evolving scientific world, the demand for portable electronics and E- vehicles has grown exponentially. However, these technologies rely heavily on efficient energy storage devices that can store and deliver energy on demand [1]. Traditional batteries have limitations in terms of their energy density, charging time and cycle life, which has sparked the search for alternative solutions. Supercapacitors have emerged as a promising solution to address the limitations of conventional batteries [2]. Unlike batteries, which rely on chemical reactions, supercapacitors store energy electrostatically, allowing for rapid charge and discharge cycles. This unique characteristic makes them ideal for applications requiring high power delivery and frequent cycling [3]. Supercapacitors utilize high surface area materials, such as activated carbon, to maximize capacitance and energy storage. Supercapacitors employ electrolytes to facilitate the movement of ions between the electrodes, which is crucial for charge storage. The choice of electrolyte affects the ionic conductivity and overall performance of the supercapacitor. Advanced research focuses on developing electrolytes with high conductivity and stability to enhance energy storage capabilities [4].

Hybrid supercapacitors combine the advantages of electrochemical double-layer capacitors (EDLCs) and pseudocapacitors. EDLCs store charge at the electrode-electrolyte interface, while pseudocapacitors involve fast and reversible faradaic reactions. By integrating both mechanisms, hybrid supercapacitors offer increased energy and power densities compared to traditional supercapacitors [5]. Graphene is a two-dimensional carbon allotrope with exceptional electrical conductivity, a high surface area and mechanical strength, which makes it an ideal candidate for supercapacitor applications [6]. Graphene-based supercapacitors have gained significant attention due to their potential for high power density, fast charge/discharge rates, long cycling life, and environmental sustainability. The field of graphene-based supercapacitors is actively researched, focusing on optimizing electrode design, exploring new graphene synthesis methods and improving the overall performance of these devices [7].

Polyaniline (PANI) is another material widely explored for its potential in supercapacitor applications [8]. It is a conducting polymer that exhibits excellent electrical conductivity, high stability, and good redox activity, making it suitable for energy storage devices. Research efforts are focused on optimizing the synthesis

methods of polyaniline, exploring different dopants and composites to enhance its performance, and investigating scalable manufacturing processes [8, 9]. A graphene-polyaniline hybrid composite has gained significant interest in the field of supercapacitors due to its synergistic effects and enhanced performance compared to individual components [10]. Graphene-PANI based supercapacitors hold promise for a wide range of applications, including portable electronics, energy storage systems, and electric vehicles, due to their enhanced performance, high power density and long cycle life. The combination of graphene, polyaniline (PANI), and ternary metal oxides in supercapacitors has also gained attention for its potential in achieving high-performance energy storage devices. [11] demonstrated a new strategy for supercapacitor formation using graphene oxide and manganese dioxide nanocomposites. The interactions between GO and MnO_2 improve the performance of the composites, highlighting the potential of these nanocomposites [12] investigated the electrochemical performance of MnO_2/g-C_3N_4/rGO nanosheets. The ternary composite material has superior performance compared to pure and binary electrode materials due to its high surface area. MnO_2/g-C_3N_4/rGO and activated carbon electrodes were used to assemble a pouch-type supercapattery device, resulting in a high energy density and self-discharging time [13] synthesized rGO-TiO_2-MoO3, an active electrode material for high-performance supercapacitors and electrochemical performance was estimated through cyclic voltammetry and galvanostatic charge-discharge studies. The composite's specific capacitance value was 472 F/gat. A composite material was prepared for supercapacitor applications, consisting of α-Manganese dioxide coated with polyaniline and reduced graphene oxide [14]. The composite showed a specific capacitance of 261 F g^{-1} and specific energy of 11 W h kg^{-1}. A one-step hydrothermal method [15] was used to synthesize a composite with MnO_2 nanowires, resulting in a synergistic effect for better energy storage performance. The synthesized nanocomposite with a 1:4 M ratio exhibits a high surface area, pore size distribution, specific capacitance, energy density, and power density. In this study, we have developed PANI-GO/MnO_2/MoO_3 nanocomposites through the hydrothermal method and investigated their structural, morphological and electrochemical performance for supercapacitor applications.

2. Materials and Method

2.1 Materials

In this study, the following chemicals were used to synthesize the samples as received from a chemical company without any other purification method: ammonium peroxo aisulfate, aniline, manganese oxide (MnO_2) and molybdenum trioxide (MoO_3).

2.2 Experimental Methods

For the experiment, we combined 0.2 M of aniline with 3 mL of HCl (1 mol) and 3 mL of citric acid in 100 mL of water to prepare the solution. The solution was then stirred for 30 minutes. Following this, 1.141 g (0.1 mol) of ammonium peroxo disulfate was slowly added, which resulted in the formation of a green-colored precipitate. The mixture was further stirred for 24 hours to ensure a complete reaction and product formation. The resulting precipitate was then washed multiple times with ethanol to remove impurities. In sample 2, 0.1 mol of polyaniline was combined with a ternary composite of GO:MnO_2/MoO_3/MnO_2 (graphene oxide) as described in our previous report [16,17]. Similarly, samples 3, 4, and 5 were prepared with 0.3 mol, 0.5 mol, and 0.7 mol of polyaniline, respectively, along with the same ternary composite. The final samples were named as follows: (a). Polyaniline, (b). 0.1m of PANI-GO:MnO_2/MoO_3, (c). 0.3 m of PANI-GO:MnO_2/MoO_3 (d). 0.5m of PANI-GO:MnO_2/MoO_3 (e). 0.7 m of PANI-GO:MnO_2/MoO_3.

2.3 Characterization Techniques

X-ray diffraction (XRD) analysis was performed using D/MAX-2500/PC and the presence of functional groups was studied by Fourier transform infrared spectroscopy (FTIR) using Perkin Elmer Spectrum 2. The surface morphology was examined using a Field Emission Scanning Electron Microscope (FESEM) using a Carl Zeiss- Sigma 300. The supercapacitor performance of electrode materials was investigated using the CHI660C model.

3. Result and Discussion

The X-ray diffraction (XRD) patterns of as-prepared ternary composites of PANI-GO:MnO_2/MoO_3 are presented in figure 1. XRD studies revealed the structural properties and phase behavior of ternary composites, aiding in understanding the synergistic effects and optimizing properties for specific functionalities. The XRD peaks of PANI were typically broad and diffuse, indicating its amorphous crystalline nature. It does not have well-defined peaks like crystalline materials. However, some peaks ranging from 25° to 28°, 31° to 34° and 36° to 39° were ascribed to PANI [18]. The lack of long-range order and disorder prevents the formation of well-defined peaks in PANI's XRD pattern. The most significant characteristic peaks of MoO_3 were observed at 18.9°, 23.0°, 24.4°, 27.1°, 28.5°, 32.0°, 37.7°, 39.3° and 43.3° which are attributed to (002), (100), (101), (110), (103), (200), (201), (202), and (211) and matched with the JCPDS card no. 21-0569 (hexagonal phase) [19,20]. Similarly, MnO_2 characteristic peaks were observed and it is worthy to note that several MnO_2 peaks were merged with MoO_3 peaks at 12.94°, 18.34°, 28.78°, 37.66°, 42.14°, 49.90°, 56.44°, 60.26°, and 69.74°.

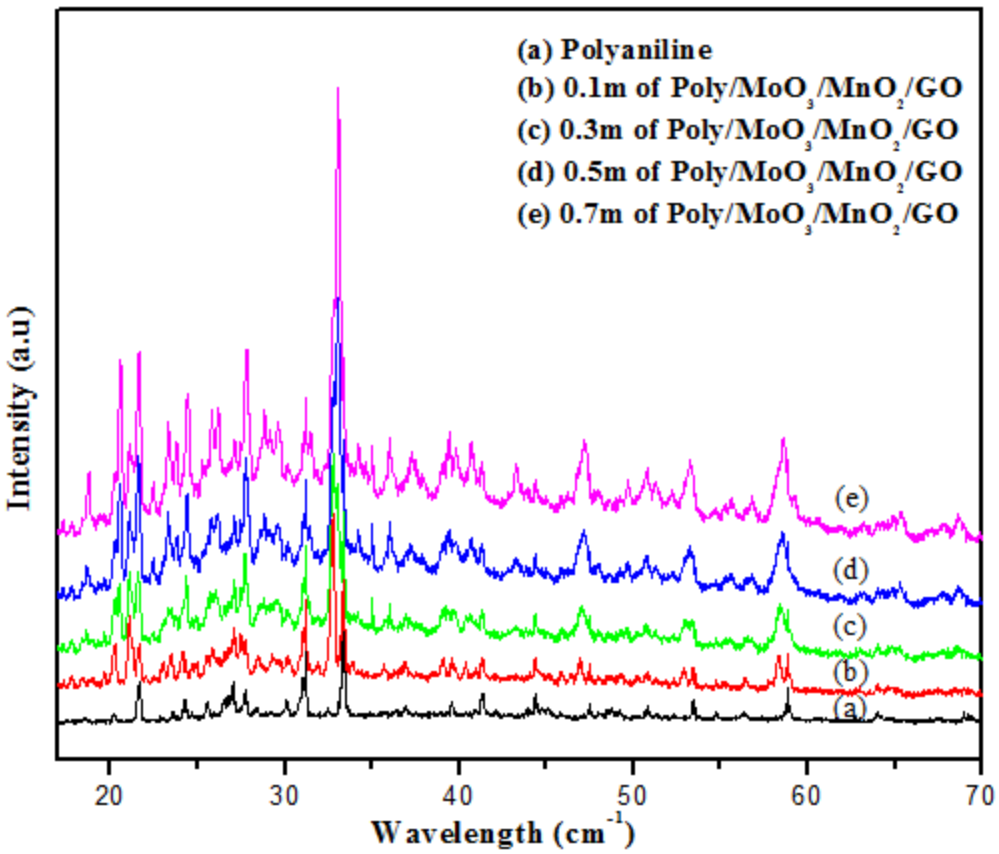

Figure 1. XRD patterns of PANI (a) and PANI-GO:MnO2/MoO3 composites (b-e)

which represent that composites were well mixed with each other and formed ternary nanocomposites [21]. The presence of graphene in the XRD pattern is very weak, and its peaks are often broad due to the limited size of graphene domains and the presence of defects.

As a result, the peaks are challenging to observe and identify in standard XRD measurements [22]. The XRD patterns of ternary composites can vary significantly depending on the composition, synthesis method and preparation conditions. Each component (PANI, MoO_3, MnO_2, and GO) contributes to the diffraction peaks. In order to explore more about the morphology of the composite and investigate the phase or chemical bonding between the components, additional techniques like Fourier-transform infrared spectroscopy (FTIR) and scanning electron microscopy (SEM) were conducted.

The presence of various chemical compositions was studied by FTIR analysis and presented in Figure 2. The Mo-O stretching vibration, a characteristic feature of MoO_3, was observed in the FTIR spectrum of the ternary nanocomposite at approximately 800-1000 cm^{-1}. This peak serves as a strong indication of the presence of MoO_3 in the nanocomposite and reflects the bond between molybdenum (Mo) and oxygen (O) atoms within the material[23]. Similarly, the FTIR spectrum also exhibited a peak corresponding to the Mn-O stretching vibration at around 600-700 cm^{-1} that confirmed the presence of MnO_2 in the nanocomposite. This peak signifies the bonding between manganese (Mn) and oxygen (O) atoms within MnO_2 Moreover, a distinctive Mo=O stretching vibration peak was detected at approximately 900-1000 cm^{-1} in the nanocomposites spectrum [24, 25]. This peak further validates the presence of MoO_3 and indicates the existence of a double bond between molybdenum (Mo) and oxygen (O) atoms within the MoO_3 component of the nanocomposites. The Mn=O stretching vibration peak was identified in the nanocomposite's spectrum at around 500-600 cm^{-1}, confirming the presence of MnO_2 in the ternary nanocomposites. This peak indicates the double bond between manganese (Mn) and oxygen (O) atoms within the MnO_2 component of the nanocomposites [24-26].

PANI typically exhibited specific peaks related to its chemical structure, such as aromatic C-H stretching vibrations around 3000-3100 cm^{-1}, C=C stretching vibrations at approximately 1530-1600 cm^{-1}, C=N stretching vibrations around 1430-1480 cm^{-1}, and N-H bending vibrations around 1560-1630 cm^{-1} [27-29]. Graphene oxide (GO) characteristic peaks related to its oxygen functional groups were observed at 3200-3600 cm^{-1}, 1720-1740 cm^{-1} and 1050-1250 cm^{-1} which were attributed to O-H stretching vibration, C=O stretching vibration and C-O stretching vibrations [30,31].

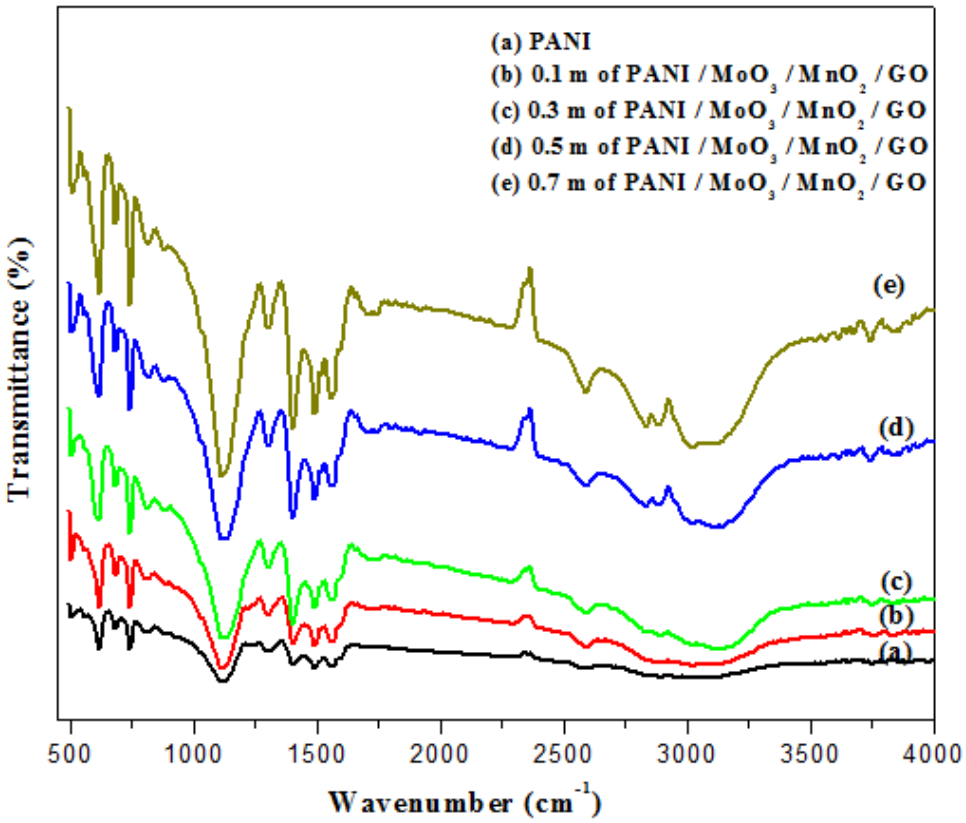

Figure 2. shows the FTIR analysis of PANI (a) and PANI-GO:MnO_2/MoO_3 composites (b-e)

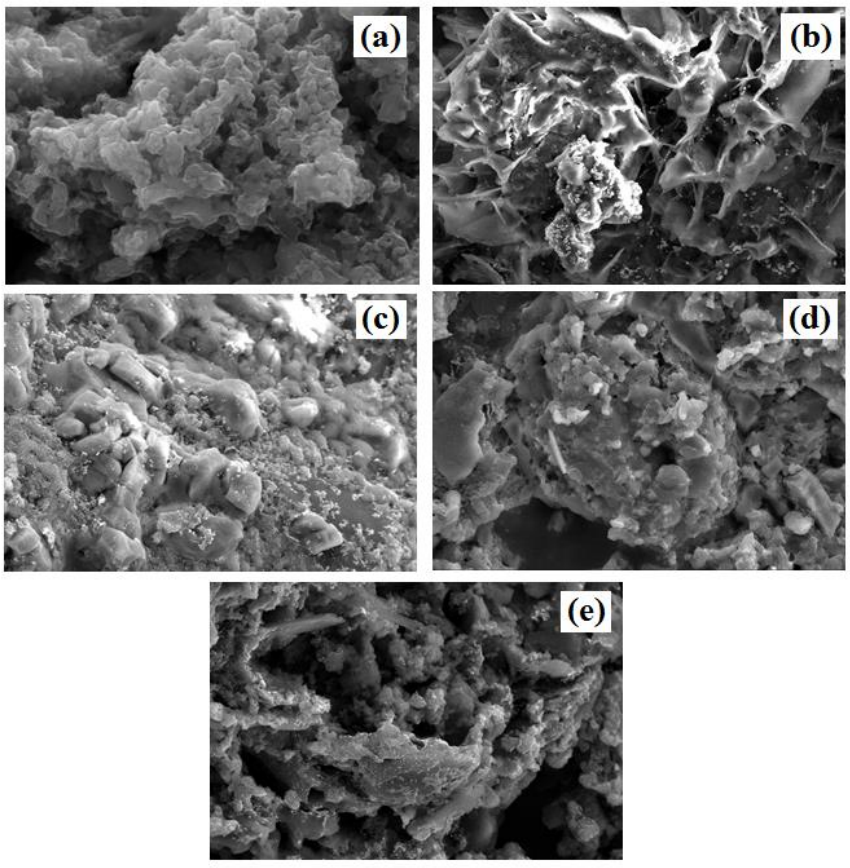

Figure 3. shows the FEMSEM images of PANI (a) and PANI-GO:MnO_2/MoO_3 composites (b-e)

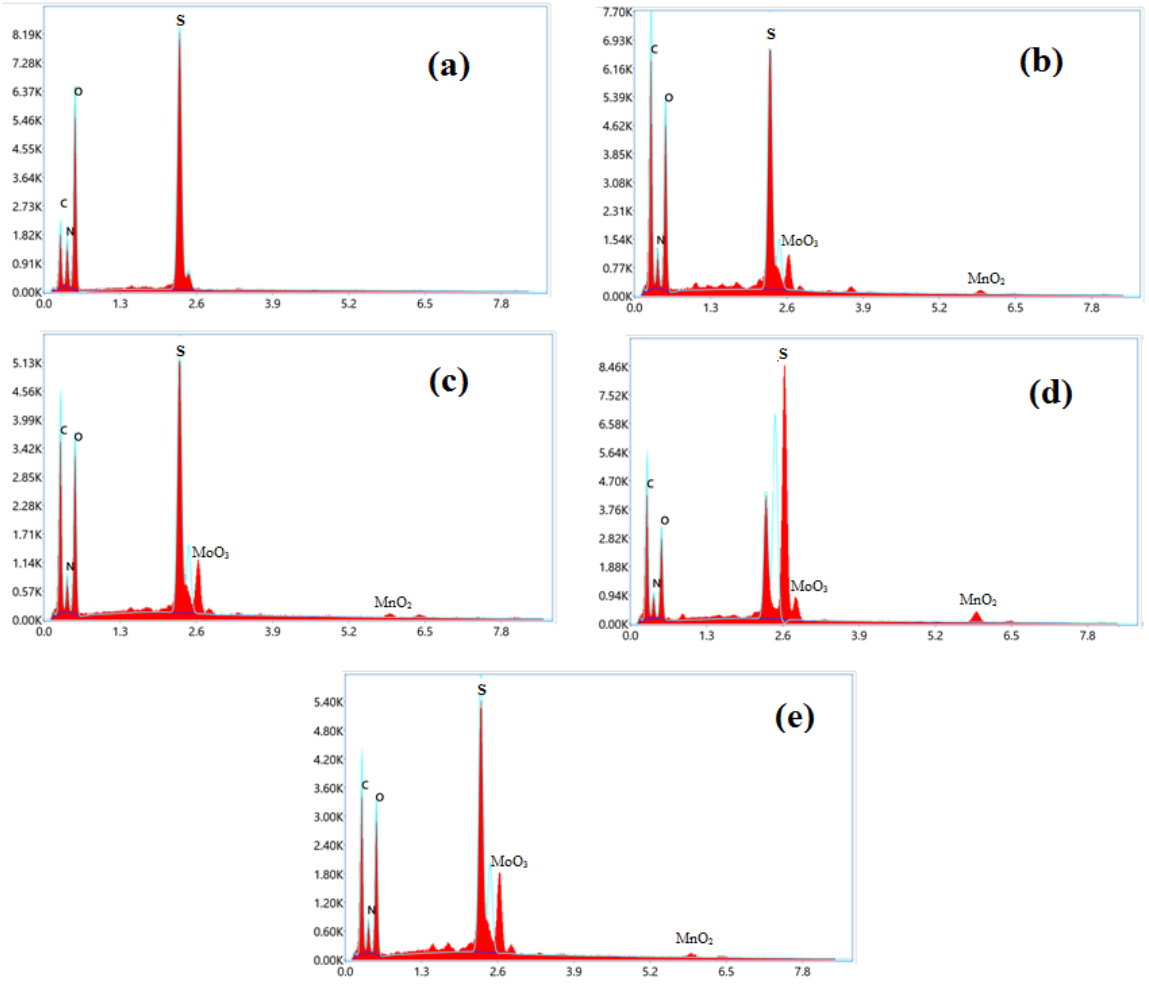

Figure 4. shows EDAX spectrum of PANI (a) and PANI-GO:MnO2/MoO3 composites (b-e)

Notably, by comparing the peaks corresponding to MoO_3 and MnO_2 in the nanocomposite spectrum to their individual spectra, significant shifts and changes were observed. These shifts suggest possible interactions and bonding between MoO_3 and MnO_2 within the ternary nanocomposite [21]. The presence of such interactions indicates the occurrence of synergistic effects within the nanocomposite, which could lead to enhanced properties and unique functionalities compared to the individual constituent materials. The FTIR analysis of the ternary nanocomposite, PANI-GO:MnO_2/MoO_3, provided valuable insights into the characteristic M-O stretching vibrations and the presence of MoO_3, MnO_2, and graphene oxide (GO) components. The observed peaks and shifts within the spectrum confirmed the presence of the individual constituents and indicated possible synergistic effects among PANI, MoO_3, MnO_2, and GO.

Figure 3 shows FESEM images of PANI (a), (b) 0.1m of PANI-GO:MnO_2/MoO_3, (c) 0.3 m of PANI-GO:MnO_2/MoO_3, (d) 0.5m of PANI-GO:MnO_2/MoO_3, and (e) 0.7 m of PANI-GO:MnO_2/MoO_3. FESEM microscopic analysis revealed that pure PANI exhibited amalgamation morphology. The amalgamation of corrugated graphene oxide layers is discernible, attributable to Van der Waals interactions facilitated by the oxygen-containing functional groups, namely carbonyl, carboxyl, epoxide, and hydroxyl groups, present on the material's surface. However, upon incorporation of ternary composites, a subtle transformation in morphology was observed, manifesting as leaf-like structures. This alteration indicated the infiltration of PANI into the ternary composites, introducing a porous nature. The rippled graphene layers host MoO_3/MnO_2 nanoparticles, strategically positioned either between or on the layers. The dispersion of these metal oxide nanoparticles on the graphene sheets serves to mitigate the tendency of graphene sheets to undergo excessive restacking. The expeditious polymerization process induces crosslinking among polyaniline chains, giving rise to the development of a porous hydrogel structure. The porous structure was anticipated to facilitate electrochemical ion intercalations, thereby contributing to enhanced electrochemical performance. Additionally, EDAX analysis validated the existence of MoO_3 and MnO_2 elements in the prepared samples, as shown in figure 4.

The electrochemical performances of the as-prepared samples were conducted on a 1 M H_2SO_4 electrode to evaluate their suitability for supercapacitor application. The electrochemical performances of the as-prepared samples were conducted on a 1 M H_2SO_4 electrode to evaluate their suitability for supercapacitor application. The cyclic voltammogram of the as-prepared ternary composite was examined over a scan rate range of 5 to 200 mV/s to explore the influence of varying scan rates (Figure.5). The cyclic voltammetry (CV) curves show the electrochemical double layer and slight pseudo-capacitive behavior. At the lower scan rate, the curves were narrow rectangular shapes, whereas at the higher scan rate, their structures deformed and got broader, which demonstrated fast electrochemical ion intercalation at the lower scan rate and slower ion intercalation at the higher scan rate [16]. This is attributed instability of electrode materials at a higher scan rate. It aligns with the generation of polaronic emeraldine from the leucoemeraldine phase, while the second redox peak arises from the transformation of polaronic emeraldine into the bipolaronic pernigraniline phase [32]. The remarkable electrochemical performance of the ternary PANI-GO:MnO_2/MoO_3 composites was a result of the harmonious synergy among all three components, leading to a well-arranged nanostructure [16, 17]. Furthermore, PANI can substantially enhance pseudo-capacitance, thereby contributing to enhanced overall capacitance. The specific capacitance of the as-prepared electrode materials was calculated as 540 F/g (b), 575 F/g for (c), 584 F/g for (d) and 596 F/g for (e) samples. Lower scan rates afford ions in the electrolyte ample time to permeate and interact with a greater surface area of the electrode, consequently yielding a heightened specific capacitance. The concurrent existence of polyaniline on GO/MnO_2/MoO_3 supports expedites electrolyte penetration, minimises charge transfer distances, and facilitates ion permeation [17].

The electrochemical impedance spectroscopy (EIS) data for PANI-GO:MnO_2/MoO_3 composites were examined through Nyquist plots in Figure 6 within a frequency range of 0.01 Hz to 100 kHz. It illustrates the change in the imaginary part of impedance (Z") plotted against the real part (Z').

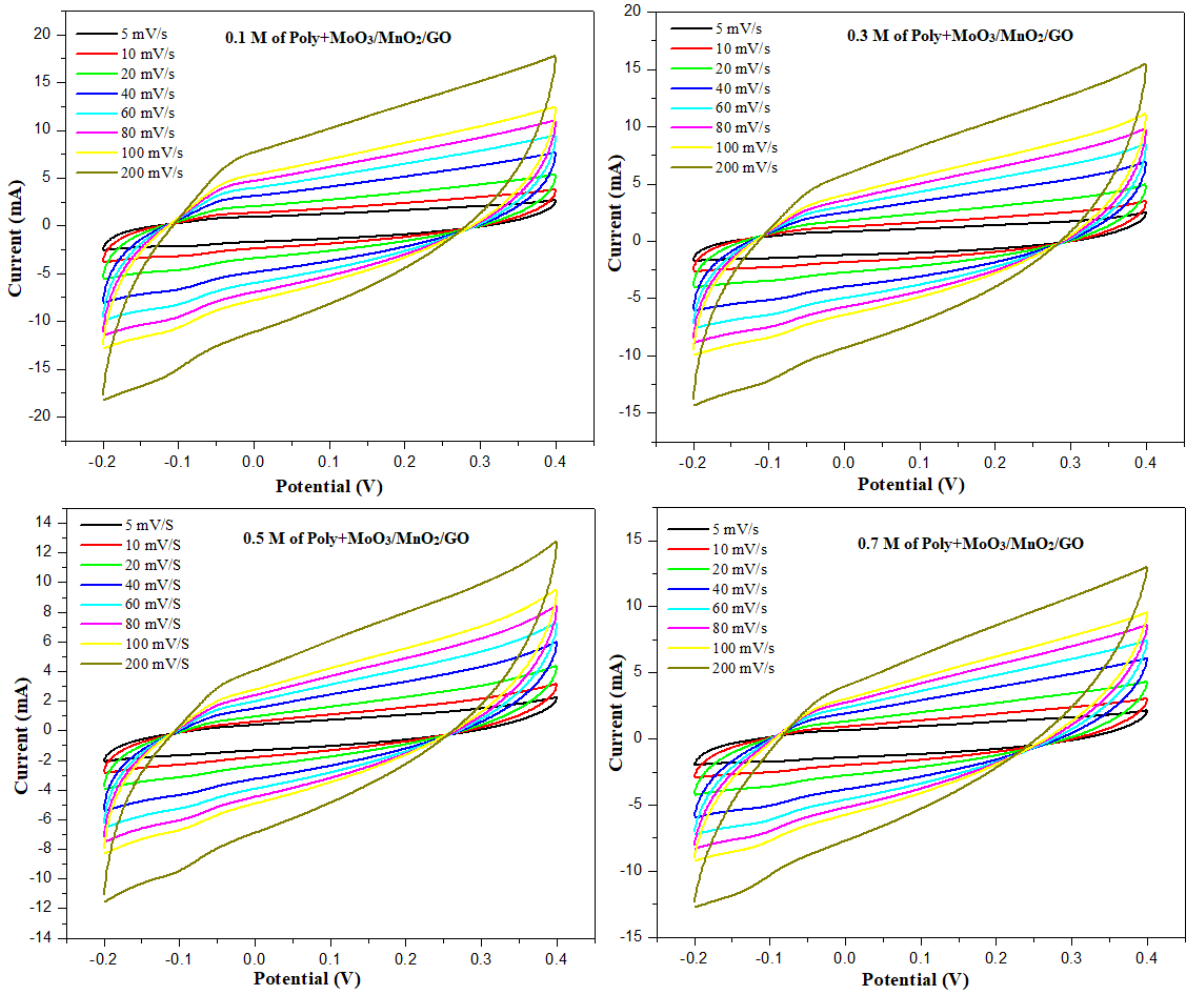

Figure 5. Cyclic voltammetry curves of PANI-GO:MnO_2/MoO_3 composites

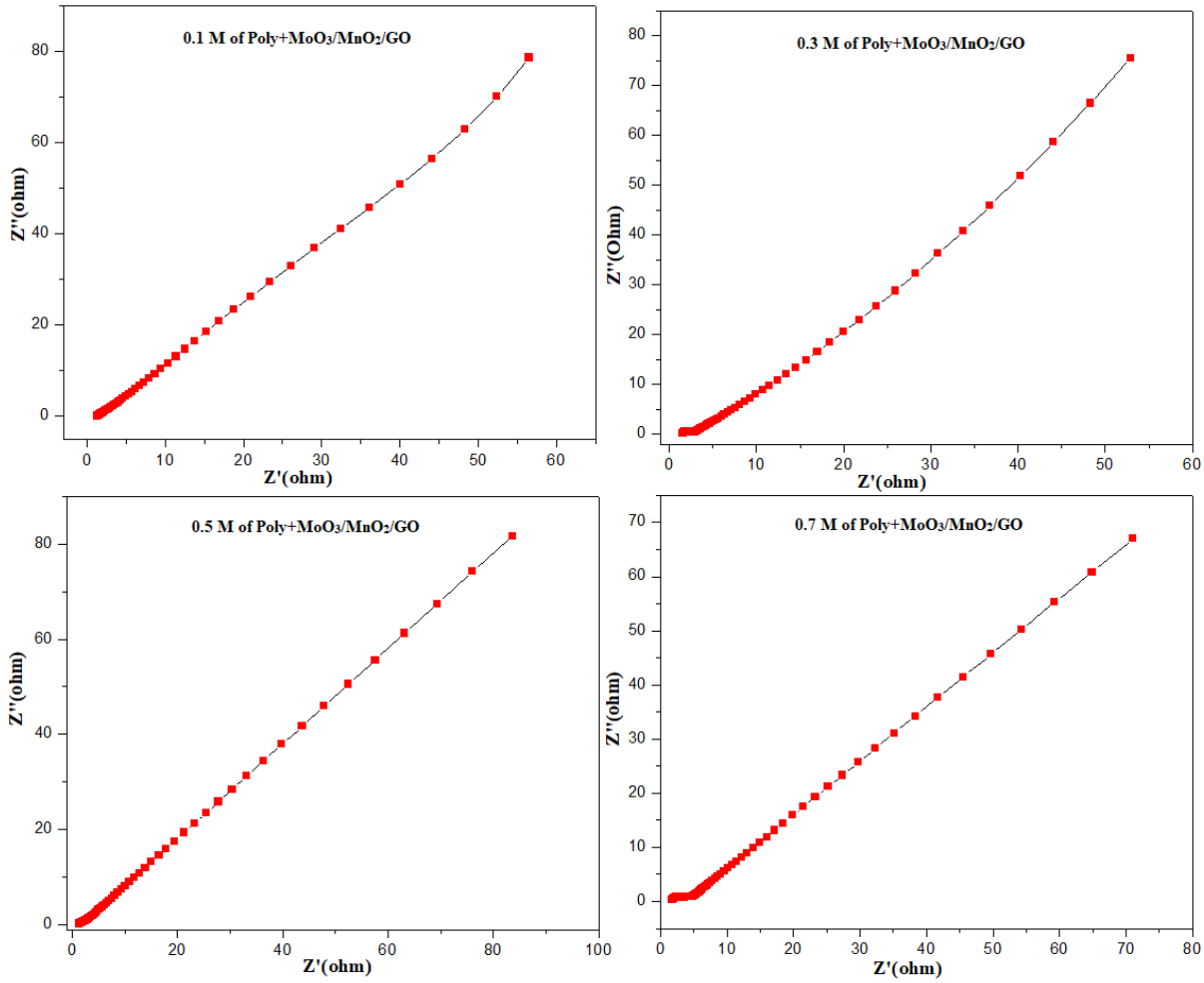

Figure 6. EIS of PANI-GO:MnO2/MoO3 composites

Each data point within the Nyquist plots corresponds to a specific frequency, and the lower left segment of the plot pertains to higher frequencies. Lower frequencies exhibit a more vertical curve, indicating ideal capacitor behavior, while higher frequencies reflect the influence of the charge-transport process on the impedance spectrum. Conversely, the low-frequency region predominantly characterizes the mass-transport process. The relative importance of each transport process hinges on the steady-state potential during the EIS measurement [33].

The Nyquist plot distinctly delineates three regions. The pronounced vertical curve at low frequency signifies capacitive behavior in the assembled cell. At higher frequencies, the cell's power capability, denoting its charge/discharge rate, is determined by the intersection of the curve at the x-axis, denoted by the equivalent series resistance (ESR) or charge transfer resistance (Rct). In the mid-frequency range, the slope of the 45° segment of the curve arises from the frequency-dependent ion transport/diffusion in the electrolyte, recognized as Warburg resistance. This reflects the impact of distributed capacitance/resistance within a porous electrode [33].

Observations reveal that, within the low-frequency range, all hydrogel samples exhibit nearly vertical lines along the -Z''-axis, indicative of preferentially capacitive behavior.

This behavior is attributed to the reversible and rapid redox reactions involving polyaniline on GO:MnO_2/MoO_3. Conversely, in the high-frequency range, the bulk resistance (Rb) is depicted by the intercept at the Z'-axis. This resistance arises from contact resistance at the interface between the active material and current collector, the ionic resistance of the electrolyte, and the intrinsic resistance of the substrate or active material. The appearance of a semicircle from the high to mid-frequency region is a consequence of the charge-transfer resistance (Rct) occurring at the electrode/electrolyte interface [34].

For ternary composite PANI-GO:MnO_2/MoO_3, the recorded values for Rct, Rb, and the overall resistance (R) at 10 mHz are 0.6, 0.5, and 5.873 Ω, respectively. As frequencies increase, both the capacitance and resistance of a porous electrode decline.

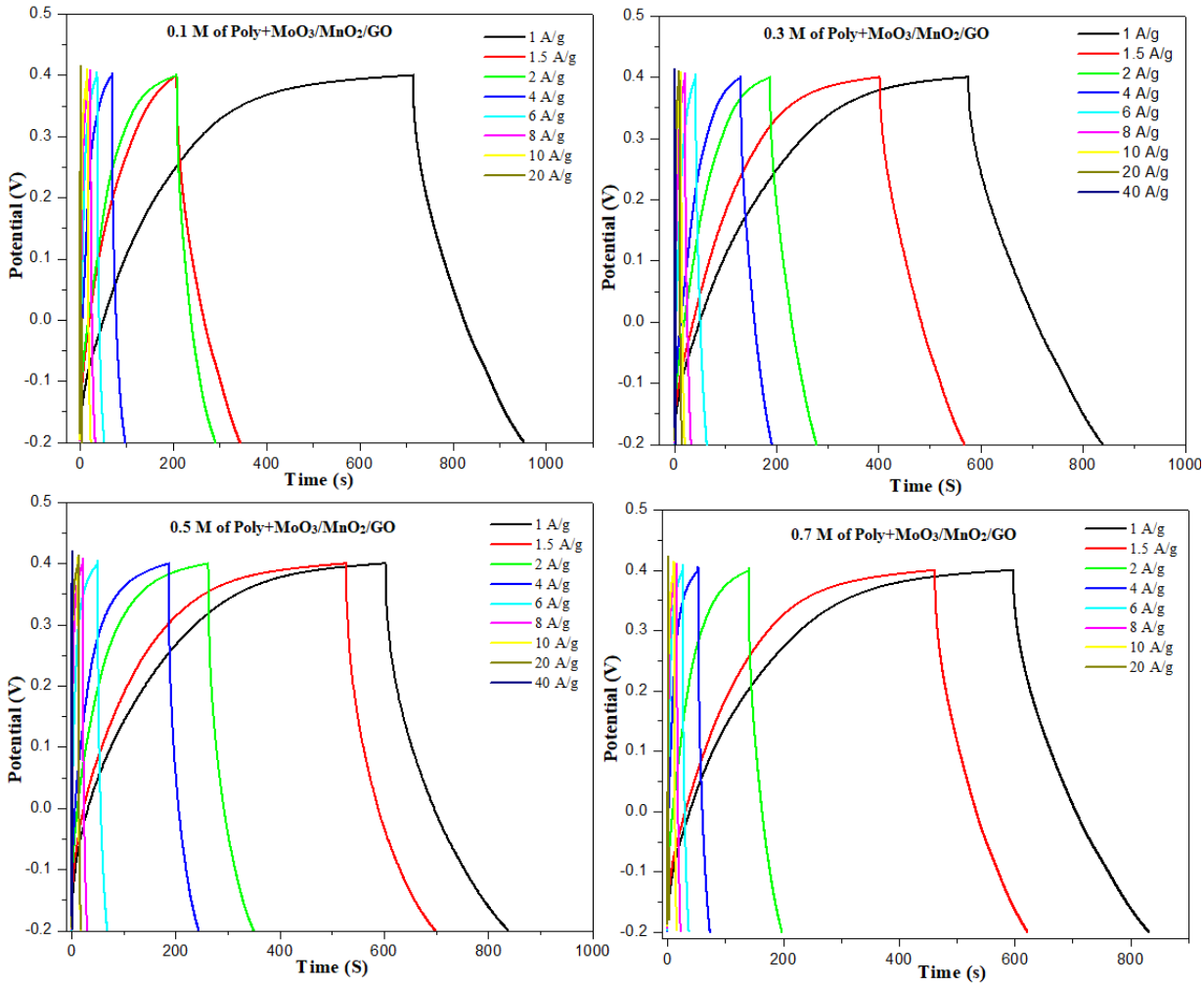

Figure 7. GCD curves of PANI:GO/MoO3/MnO2 composites

This phenomenon occurs because, at higher frequencies, only a portion of the active porous layer is accessible. The capacitor's rate performance can be assessed through the response time (τ_0), defined as the reciprocal of the response frequency (f_0) at which the phase difference between the real and imaginary components of impedance is 45°, and the resistive and capacitive influences on the total impedance are equal [32-34].

Figure 7 illustrates the charging-discharging plots of as-prepared electrodes at a constant current density of 0.25 A/g. Evidently, the charging-discharging times vary among different samples at the consistent current density, indicating distinct specific capacitances. The discharging time increases with the concentration of PANI for various samples, and the GO:MnO_2/MoO_3 composite exhibits the longest discharging time, consequently resulting in the highest specific capacitance. The nearly linear and symmetric charge-discharge plots indicate the favorable capacitive behavior of Electric Double-Layer Capacitor (EDLC) and Faradic capacitance for these hydrogel electrodes. All discharge curves exhibit two voltage steps, initially a rapid IR drop attributed to the internal resistance of the cell, followed by a gradual voltage decay associated with the pseudo capacitive behavior of the electrodes [35, 36]. The deviation from linearity underscores that the primary contribution to capacitance stems from the redox reactions involving polyaniline and GO:MnO_2/MoO_3 species. The enhanced interconnectivity facilitated by polyaniline within the GO:MnO_2/MoO_3 and graphene promotes a charge storage mechanism through redox reaction-based pseudo capacitance.

4. Conclusion

In conclusion, our study on PANI-GO:MnO_2/MoO_3 nanocomposites for supercapacitor applications reveal promising prospects in addressing the growing energy storage needs of contemporary technologies. The study investigates the potential of PANI-GO:MnO_2/MoO_3 nanocomposites as high-performance supercapacitor. It combines polyaniline (PANI) with a ternary composite of GO/MoO_3/MnO_2 to improve electrochemical performance. XRD analysis confirms the hexagonal phase, FTIR shows functional

groups, FESEM images show leaf-like structures, and EDAX spectrum confirms Mn and Mo elements. The nanocomposites exhibited the maximum capacitance of 596 F/g. The research aims to understand how different levels of polyaniline impact the overall composition and their effects on energy storage capabilities. By varying the polyaniline content alongside a ternary composite of MoO_3/MnO_2/GO, we have gained valuable insights into the intricate interplay of these components and their collective impact on electrochemical performance.

References

[1] C. Liu, F. Li, M. Lai-Peng, H.M. Cheng, Advanced materials for energy storage. Advanced Materials, 22(8), (2010) E28-62. https://doi.org/10.1002/adma.200903328

[2] P. Simon, Y. Gogotsi, Materials for electrochemical capacitors. Nature Materials, 7(11), (2008) 845–854. https://doi.org/10.1038/nmat2297

[3] B. Pal, S. Yang, S. Ramesh, V. Thangadurai, R. Jose, Electrolyte selection for supercapacitive devices: a critical review. Nanoscale Advances, 1(10), (2019) 3807–3835. https://doi.org/10.1039/C9NA00374F

[4] B.E. Conway, (1999) Electrochemical Supercapacitors. Electrochem. Springer, New York. https://doi.org/10.1007/978-1-4757-3058-6

[5] P. Periasamy, T. Krishnakumar, M. Sandhiya, M. Sathish, M. Chavali, P.F Siril, V.P. Devarajan, Electrochemical investigation of hybridized WO 3–CdS semiconducting nanostructures prepared by microwave-assisted wet chemical route for supercapacitor application. Journal of Materials Science: Materials in Electronics, 30(10), (2019) 9231-9244. https://doi.org/10.1007/s10854-019-01252-w

[6] P. Periasamy, T. Krishnakumar, M. Sathish, M. Chavali, P. F. Siril, V.P. Devarajan, Structural and electrochemical studies of tungsten oxide (WO<inf>3</inf>) nanostructures prepared by microwave assisted wet-chemical technique for supercapacitor. Journal of Materials Science: Materials in Electronics, 29(8), (2018) 6157–6166. https://doi.org/10.1007/s10854-018-8590-6

[7] T. Kim, H.C.Kang, T.T. Tung, J.D. Lee, H. Kim, W.S. Yang, H.G. Yoon, K.S. Suh, Ionic liquid-assisted microwave reduction of graphite oxide for supercapacitors. RSC Advances, 2(23), (2012) 8808-8812. https://doi.org/10.1039/C2RA21400H

[8] M.M. Rahman, M.R. Hossen, I. Alam, M.H. Rahman, O. Faruk, M. Nurbas, M.M. Rahman, M.M.R. Khan, Synthesis of hexagonal boron nitride based PANI/h-BN and PANI-PPy/h-BN nanocomposites for efficient supercapacitors. Journal of Alloys and Compounds, 947, (2023) 169471. https://doi.org/10.1016/j.jallcom.2023.169471

[9] H. Hamedani, A.K. Ghasemi, M.S. Kafshgari, Y. Zolfaghari, L.A. Kafshgari, Electrochemical performance of 3D porous PANI/Gr/MIL-100(Fe) nanocomposite as a novel smart supercapacitor electrode material. Synthetic Metals, 298, (2023) 117428. https://doi.org/10.1016/j.synthmet.2023.117428

[10] P. Haldar, S. Biswas, V. Sharma, A. Chowdhury, A. Chandra, Mn3O4-polyaniline-graphene as distinctive composite for use in high-performance supercapacitors. Applied Surface Science, 491, (2019) 171–179. https://doi.org/10.1016/j.apsusc.2019.06.106

[11] R.R. Kumar, S. Thanigaivel, A.K. Priya, A. Karthick, C. Malla, P. Jayaraman, M. Muhibbullah, R.A. Alshgari, A.M. Karami, Fabrication of MnO2 Nanocomposite on GO Functionalized with Advanced Electrode Material for Supercapacitors. Journal Nanomaterials, (2022) 7929270. https://doi.org/10.1155/2022/7929270

[12] R. Kumar, R. Thangappan, Synergetic effect on enhanced electrochemical properties of MnO2 nanorods on g-C3N4/rGO nanosheet ternary composites for pouch-type flexible asymmetric supercapattery device. Journal of Energy Storage, 70, (2023) 108149. https://doi.org/10.1016/j.est.2023.108149

[13] S. Britto, V. Ramasamy, P. Murugesan, R. Thangappan, R. Kumar, Preparation and electrochemical validation of rGO-TiO2-MoO3 ternary nanocomposite for efficient supercapacitor electrode. Diamond and Related Materials, 122, (2022) 108798. https://doi.org/10.1016/j.diamond.2021.108798

[14] P.H. Patil, V.V. Kulkarni, T.D. Dongale, S.A. Jadhav, α-Manganese Dioxide (α-MnO2) Coated with Polyaniline (PANI) and Reduced Graphene Oxide (rGO)-Based Nanocomposite for Supercapacitor Application. Journal of Composites Science, 7, (2023) 167. https://doi.org/10.3390/jcs7040167

[15] D. Sahoo, J. Shakya, S. Choudhury, S.S. Roy, L. Devi, B. Singh, S. Ghosh, B. Kaviraj, High-performance MnO2 Nanowire/MoS2 nanosheet composite for a symmetrical solid-state supercapacitor. ACS omega, 7, (2022) 16895-16905. https://doi.org/10.1021/acsomega.1c06852

[16] R. Kalpana, S. Ashokan, P. Subbaramaniyan, P. Shanmugasundaram, D. Sudha, S. Thennarasu, J. Jesbin, Preparation and Characterization of Graphene Doped Molybdenum Trioxide/Manganese Oxide Ternary Nanocomposite for Supercapacitor Performance. Brazilian Journal Physics, 51(6), (2021) 1597–1602. https://doi.org/10.1007/s13538-021-00940-5

[17] R. Kalpana, P. Subbramaniyan, Enhancing Surface Area, Electrochemical Performance, and Morphological Properties of MoO3/GO/MnO2 Ternary Nanocomposites through Annealing Temperature Optimization. Journal of Electronic Materials, 53(2), (2023) 1002–1011. https://doi.org/10.1007/s11664-023-10859-z

[18] S. Shahabuddin, N.M. Sarih, S. Mohamad, J.J. Ching, SrTiO3 Nanocube-Doped Polyaniline Nanocomposites with Enhanced Photocatalytic Degradation of Methylene Blue under Visible Light. Polymers, 8(2), (2016) 27. https://doi.org/10.3390/polym8020027

[19] X. Wan, S. Yang, Z. Cai, Q. He, Y. Ye, Y. Xia, G. Li, J. Liu, Facile synthesis of MnO2 nanoflowers/N-doped reduced graphene oxide composite and its application for simultaneous determination of dopamine and uric acid. Nanomaterials, 9(6), (2019) 847. https://doi.org/10.3390/nano9060847

[20] S. Bai, C. Chen, R. Luo, A. Chen, D. Li, Synthesis of MoO3/reduced graphene oxide hybrids and mechanism of enhancing H2S sensing performances. Sensors and Actuators B: Chemical, 216, (2015) 113–120. https://doi.org/10.1016/j.snb.2015.04.036

[21] P.M. Shafi, R. Dhanabal, A. Chithambararaj, S. Velmathi, and A. C. Bose, α-MnO2/h-MoO3 Hybrid Material for High Performance Supercapacitor Electrode and Photocatalyst. ACS Sustainable Chemistry & Engineering, 5(6), (2017) 4757–4770. https://doi.org/10.1021/acssuschemeng.7b00143

[22] F.T. Johra, J.W. Lee, W.G. Jung, Facile and safe graphene preparation on solution based platform. Journal of Industrial and Engineering Chemistry, 20(5), (2014) 2883–2887. https://doi.org/10.1016/j.jiec.2013.11.022

[23] B. Gowtham, V. Ponnuswamy, G. Pradeesh, J. Chandrasekaran, D. Aradhana, MoO3 overview: hexagonal plate-like MoO3 nanoparticles prepared by precipitation method. Journal of Materials Science: Materials in Electronics, 29(8), (2018) 6835–6843. https://doi.org/10.1007/s10854-018-8670-7

[24] M. Mylarappa, V.V. Lakshmi, K.R.V. Mahesh, H.P. Nagaswarupa, N. Raghavendra, A facile hydrothermal recovery of nano sealed MnO2 particle from waste batteries: An advanced material for electrochemical and environmental applications. IOP Conference Series: Materials Science and Engineering, 149(1), (2016) 012178. https://doi.org/10.1088/1757-899X/149/1/012178

[25] Y. Kumar, S. Chopra, A. Gupta, Y. Kumar, S.J. Uke, S.P. Mardikar, Low temperature synthesis of MnO2 nanostructures for supercapacitor application. Materials Science for Energy Technologies. 3, (2020) 566–574. https://doi.org/10.1016/j.mset.2020.06.002

[26] M.A. Marzouk, H.A. ElBatal, R.L. Elwan, Effect of MoO3, MnO2 or mixed dopants on the spectral properties and crystallization behavior of sodium phosphate glasses containing either MgO or MgF2. Applied Physics A, 125(6), (2019) 1–11. https://doi.org/10.1007/s00339-019-2679-5

[27] U.M. Chougale, J.V. Thombare, V.J. Fulari, A.B. Kadam, (2013) Synthesis of polyaniline nanofibres by SILAR method for supercapacitor application. International Conference on Energy Efficient Technologies for Sustainability, IEEE, India. https://doi.org/10.1109/ICEETS.2013.6533537

[28] S. Verma, V.K. Pandey, B. Verma, Facile synthesis of graphene oxide-polyaniline-copper cobaltite (GO/PANI/CuCo2O4) hybrid nanocomposite for supercapacitor applications. Synthetic Metals, 286, (2022) 117036. https://doi.org/10.1016/j.synthmet.2022.117036

[29] B. Sydulu Singu, P. Srinivasan, S. Pabba, Benzoyl Peroxide Oxidation Route to Nano Form Polyaniline Salt Containing Dual Dopants for Pseudocapacitor. Journal of the Electrochemical Society, 159(1), (2011) A6–A13. https://doi.org/10.1149/2.036201jes

[30] T.F. Emiru, D.W. Ayele, Controlled synthesis, characterization and reduction of graphene oxide: A convenient method for large-scale production. Egyptian Journal of Basic and Applied Sciences, 4(1), (2017) 74–79. https://doi.org/10.1016/j.ejbas.2016.11.002

[31] E. Andrijanto, S. Shoelarta, G. Subiyanto, S. Rifki, Facile synthesis of graphene from graphite using ascorbic acid as reducing agent. AIP Conference Proceeding, 1725 (2016). https://doi.org/10.1063/1.4945457

[32] X. Liu, P. Shang, Y. Zhang, X. Wang, Z. Fan, B. Wang, Y. Zheng, Three-dimensional and stable polyaniline-grafted graphene hybrid materials for supercapacitor electrodes. Journal of Materials

Chemistry, 2(37), (2014) 15273–15278. https://doi.org/10.1039/C4TA03077J

[33] L. Wen, K. Li, J. Liu, Y. Huang, F. Bu, B. Zhao, Y. Xu, Graphene/polyaniline@carbon cloth composite as a high-performance flexible supercapacitor electrode prepared by a one-step electrochemical co-deposition method. RSC Advances, 7(13), (2017) 7688–7693. https://doi.org/10.1039/C6RA27545A

[34] Z. Yang, L. Tang, J. Ye, D. Shi, S. Liu, M. Chen, Hierarchical nanostructured α-Fe2O3/polyaniline anodes for high performance supercapacitors. Electrochimica Acta, 269, (2018) 21–29. https://doi.org/10.1016/j.electacta.2018.02.144

[35] H. Chauhan, M.K. Singh, S.A. Hashmi, S. Deka, Synthesis of surfactant-free SnS nanorods by a solvothermal route with better electrochemical properties towards supercapacitor applications. RSC Advances, 5(22), (2015) 17228–17235. https://doi.org/10.1039/C4RA15563G

[36] B. Senthilkumar, K. Vijaya Sankar, C. Sanjeeviraja, R. Kalai Selvan, Synthesis and physico-chemical property evaluation of PANI–NiFe2O4 nanocomposite as electrodes for supercapacitors. Journal of Alloys and Compounds, 553, (2013) 350–357. https://doi.org/10.1016/j.jallcom.2012.11.122

Authors Contribution Statement

R. Kalpana - Conceptualization, Methodology, Investigation, Writing - Original Draft. P. Subbramaniyan - Supervision, Validation, Investigation, Writing - Review & Editing.

Funding

No funding was received for this work.

Conflict of Interest

We wish to confirm that there are no known conflicts of interest associated with this publication and there has been no significant financial support for this work that could have influenced its outcome.

Has this article screened for similarity?

Yes

About the License